



Shahrood University of
Technology



Iranian Society of
Mining Engineering
(IRSM)

Analysis of Granite Failure Modes and Energy Conversion under Uniaxial Compression at Various Temperatures

Kausar Sultan Shah^{1*}, Naeem Abbas^{1,2}, Li Kegang², Mohd Hazizan bin Mohd Hashim³, Hafeezur Rehman^{3,4}, and Khan Gul Jadoon¹

1. Department of Mining Engineering, Karakoram International University (KIU), Gilgit, Pakistan

2. Faculty of Land Resource Engineering, Kunming University of Science and Technology, Kunming, Yunnan, China

3. Strategic Mineral Niche, School of Materials and Mineral Resources Engineering, Universiti Sains Malaysia, Engineering Campus, Nibong Tebal, Penang, Malaysia

4. Department of Mining Engineering, Baluchistan University of Information Technology, Engineering and Management Sciences, Quetta, Pakistan

Article Info

Received 23 March 2023

Received in Revised form 21 April 2023

Accepted 30 April 2023

Published online 30 April 2023

DOI: [10.22044/jme.2023.12870.2336](https://doi.org/10.22044/jme.2023.12870.2336)

Keywords

Failure mode

Granite

Dissipated energy

Elastic energy

Axial splitting

Abstract

The rocks in the studied area are prone to deterioration and failure due to frequent exposure to extreme temperature variations and loading conditions. In the context of rock engineering reliability assessment, understanding the energy conversion process in rocks is critical. Therefore, this research work aims to assess the energy characteristics and failure modes of pink and white-black granite subjected to uniaxial compression loading at various temperatures. Samples of pink and white-black granite are heated to a range of temperatures (0 °C, 200 °C, 400 °C, 600 °C, 900 °C, and 1100 °C), and their failure modes and energy characteristics including total energy, elastic energy, and dissipated energy are studied by testing preheated samples under uniaxial compression. The results show that the dissipation energy coefficient initially rises rapidly, and then falls back to its minimum value at the failure stage. The microstructures of granite rock directly affect its elastic and dissipation energy. Axial splitting failure mode is observed in most of the damaged granite specimens. After heating granite to 600 °C, the effect of temperature on the failure mode becomes apparent.

1. Introduction

Geo-technical engineering deals with various problems related to fields such as mining, civil, and petroleum engineering [1-5]. These problems are related to ground stability in underground mines, foundation design, earthworks, embankments, and wellbore stability [6-8]. In geo-technical engineering, the mechanical behavior of rocks is a crucial aspect in addressing these problems. Energy variation is a complex phenomenon in geo-technical constructions, particularly in underground mines, involving input energy, absorption, accumulation, dissipation, and release [9]. Therefore, investigating energy conversion in rocks under uniaxial compression is critical because it substantially impacts the safety and stability of rock engineering projects.

The deformation and failure process of rocks is a complex and gradual damage evaluation process that is triggered by energy [10]. A thorough understanding of energy evaluation is required to comprehend the deformation and failure process of rock. Several significant research works on energy variation during deformation and rock failure has been conducted across a broad spectrum of rock mechanics applications. He *et al.* [10] investigated the various forms of energy and dissipation energy coefficient during rock failure for fifteen different rocks, and proposed a new approach for estimating rock deformation based on the dissipation energy coefficient. Their findings showed that the dissipation energy coefficient increased linearly during the compaction stage but decreased at the yield and peak stages. Cao *et al.* [11] evaluated the

✉ Corresponding author: kausar.sultan@kiu.edu.pk (K.S. Shah)

strain energy of water-saturated sandstone using infrared radiation (IR). The authors discovered that at the peak strength, total and elastic energies were negatively correlated linearly, while dissipation energy was negatively correlated exponentially. Li *et al.* [12] conducted triaxial compression tests on granite rock under different loading and unloading modes. They showed that the total, elastic, and circumferential energy were proportional to the confining pressure. Hemmati *et al.* [13] investigated the relationship between the texture and strength properties (uniaxial compression strength (UCS) and Brazilian tensile strength (BTS) tests) of granite rock. The authors demonstrated that the recently developed quartz-to-feldspar size ratio (QFSR) indicator has a substantial correlation with both UCS and BTS.

Hao *et al.* [14] evaluated the dissipation energy of sandstone during failure while subjected to uniaxial cyclic loading and unloading under saturated and dry settings using acoustic emission. Water saturation enhanced the rate of dissipation energy during the final loading and unloading but inhibited the abrupt reduction in elastic energy. The findings can be used to develop experimental and predictive models for monitoring and warning of rock engineering disasters in hydraulic fractures, slopes, coal mines, and tunnels [14]. A detailed laboratory investigation of rock failure mechanisms triggered by strain energy can aid in assessing the support designed for an engineering task. Therefore, quantifying the mode of failure is essential to properly assess the deformation and failure process.

Despite the fact that the UCS test process is simple, the specimen stress concentration and fracture pattern are significantly more complex than in Brazilian and triaxial tests [15]. The literature has made an effort to explain the failure mechanism in rock subjected to uniaxial compression. Basu *et al.* [16] examined the uniaxial compression failure mechanisms of sandstone, schist, and granite. According to the study results, the failure modes of granite rock are multiple fracturing, axial splitting, and shearing along a single plane and double plane. Rocks include defects of varying sizes. Initially, the larger defects were the ones that responded most strongly to compression. Axial splitting occurs when the fracture widens without any horizontal tension.

Horizontal strains prevented the growth of these bigger cracks, and at a certain stress stage, appropriately oriented smaller cracks emerged due to their interaction. This leads to the formation of a localized area where numerous microscopic cracks can propagate and eventually cause a macroscopic collapse [17].

Previous research work has focused on the evaluation characteristics of strain energy under loading-unloading and saturated-dry conditions of rocks, whereas the effect of heating conditions of pink and white-black granite has received little attention. Therefore, this work aims to investigate the strain energy characteristics of pink and white-black granite rocks during uniaxial compression loading at different temperatures. The study findings provide an experimental basis for understanding the significance of temperature effects on the strain energy of pink and white-black granite, which governs large rock engineering disasters including mine disasters.

2. Methodology

2.1. Sample preparation and experimental setup

Pink and white-black granite rock samples were used in this work. Pink granite samples were collected in boulder form from Chilas, Gilgit, Pakistan, whereas, white-black granite specimens were taken in Sakarkoi, Gilgit. All the specimens were drilled from the boulder and shaped into 54 mm × 135 mm (diameter × height) (Figure 2) according to American Society of Testing and Materials (ASTM) D4543-08 [18]. The fundamentals properties of the test samples are detailed in Table 1. Furthermore, all white-black and pink granite specimens were heated in a heat treatment furnace to temperatures ranging from 200 to 1100 °C. The reason for adopting a temperature range of 0-1100 °C in this investigation is as follows. Many geo-technical uses can benefit from understanding how rocks react to various temperature treatments. For example, Vidana Pathiranagei *et al.* [19], Małkowski *et al.* [20], Yuan *et al.* [21], and Nahhas *et al.* [22] investigate the effect of temperature on the mechanical properties of rocks at various temperatures ranging from 25 to 1100 °C.

Table 1. Properties of white-black and pink granite of Gilgit.

Properties	White-black granite	Pink granite
UCS (MPa)	89.5	93
Tensile strength (MPa)	6.8	11.8
Porosity %	0.44	0.1
Moisture content %	0.25	0.22
Sp. Gravity g/cm ³	2.65	2.66
Velocity P wave (m/s)	2972.22	49767
Dry density g/cm ³	2.6	2.64
Schmidt hammer value	54	58
Point load index MPa	5.9	6.8

Electro-hydraulic Servo Universal Testing Machine (UTM-1000E), 1000 kN was used for the uniaxial compression testing, as shown in Figure 1. The uniaxial compression test was conducted in

adherence to the ASTM standard D 2938-95 [23]. All the specimens were tested under a loading rate of 5 kN/s.

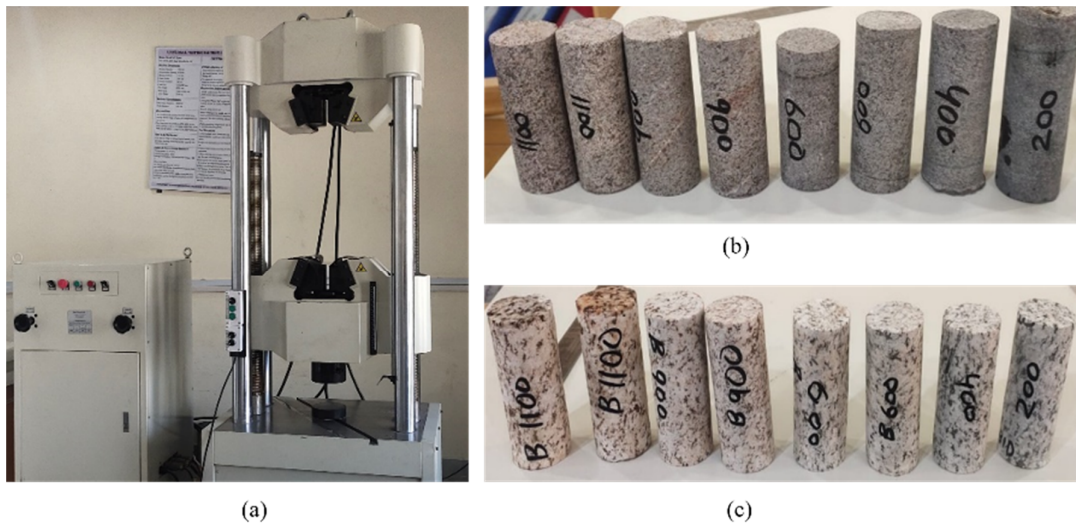


Figure 1. Experimental testing setup and granite samples (a) UTM-1000E (b) Pink granite, and (c) white-black granite.

2.2. Energy calculation

It is anticipated that no heat is lost during the deformation and failure process of rock when subjected to an external load [10, 24]. Consequently, according to the first law of thermodynamics, the following expression can be used to derive the total energy:

$$U = U^e + U^d \quad (1)$$

where (U , U_e , U_d) stands for (total, elastic, and dissipated) energies. The total energy during rock failure refers to the sum of all the energy that is dissipated or released as a result of rock failure. When a rock sample is subjected to an external load, it experiences deformation, and the energy required to produce this deformation is stored in

the rock as elastic energy, whereas the energy dissipated during rock failure refers to the energy that is absorbed and released as a result of rock breaking or fracturing. The amount of elastic energy stored in a material depends on its elastic modulus, which is a measure of its resistance to deformation, and the amount of deformation produced. In general, the more resistant a material is to deformation, the more elastic energy it can store. The relationship between elastic energy, dissipated energy, and elastic modulus is illustrated in Figure 2.

As previously discussed, Figure 2 illustrates the representation of total energy, elastic energy, and dissipated energy under the stress-strain curve, whereas the elastic energy is represented by the shaded area inside the triangle. The shaded area

between the elastic modulus line and the stress-strain curve represents dissipated energy. To compute each type of energy, the following methods were used as outlined in the references [10, 25]:

$$U = \int_0^{\epsilon_1} \sigma d\epsilon_1 \tag{2}$$

$$U^e = \frac{\sigma^2}{2E} \tag{3}$$

$$U^d = U - U^e \tag{4}$$

where E stands for the elastic modulus, and σ and ϵ denote stress and strain.

$$\lambda = \frac{U^d}{U^e} \tag{5}$$

Understanding the mechanics of rock failure involves a complex energy conversion mechanism. A key parameter that provides insight into this process is the dissipated energy coefficient, which is defined as the ratio of dissipated energy to elastic energy. This dissipated energy coefficient is an important parameter in rock failure mechanism, as it helps to elucidate the mechanism of energy transformation and dissipation [10, 11].

3. Results and Discussion

3.1. Elemental analysis

Granite is composed of various minerals including feldspar, quartz, mica, and hornblende. The physical and chemical properties of this rock

can be influenced by its elemental composition. When comparing white granite and pink granite (Table 3), pink granite is comparatively finer-grained, which means that the individual mineral grains in pink granite are smaller and more closely packed together than in white granite. Along with the size of grains, the elemental composition of granite can have a significant impact on its properties. In comparison, pink granite has a lower silica content and higher levels of iron, calcium oxide, and magnesium oxide. The presence of silica is a major component of granite that contributes to its hardness, durability, and resistance to weathering. Pink granite may have a lower silica content, which can make it less hard and durable than white granite. However, the higher iron content in pink granite can give it a unique pink, red or brown coloration that may be desirable for certain applications. Additionally, pink granite contains higher levels of calcium oxide and magnesium oxide, which are important components that can influence its physical and chemical properties. The higher levels of calcium oxide and magnesium oxide in pink granite can affect its durability and strength, while the lower levels in white granite may contribute to its hardness and resistance to weathering. In summary, when comparing the elemental analysis of pink and white granite, pink granite typically has a lower silica content and higher levels of iron, calcium oxide, and magnesium oxide. However, it is important to consider other factors, such as grain size, mineralogy, texture, and structure, when making comparisons between these two types of granite.

Table 2. XRF results of Chilas pink granite and Sakarkoi white-black granite.

Pink granite			White-black granite		
Elements	Composition	Percentage	Elements	Composition	Percentage
Silicon	SiO ₂	56.184	Silica	SiO ₂	72.04
Iron	Fe ₂ O ₃	16.681	Aluminum	Al ₂ O ₃	14.42
Calcium	CaO	13.315	Potassium	K ₂ O	4.12
Aluminum	Al ₂ O ₃	11.012	Sodium	Na ₂ O	3.69
Magnesium	MgO	2.022	Calcium	CaO	1.82
Potassium	K ₂ O	0.21	Iron	FeO	1.68
Phosphorous	P ₂ O ₅	0.107	Iron	Fe ₂ O ₃	1.22
Zirconium	ZrO ₂	0.087	Magnesium	MgO	0.71
Manganese	MnO	0.088	Titanium	TiO	0.30
Niobium	Nb ₂ O ₅	0.020	Phosphorous	P ₂ O ₃	0.12
Arsenic	As ₂ O ₅	0.022	Manganese	MnO	0.05

3.2. Energy and deformation stages

Rock is primarily damaged by the absorption, accumulation, and dissipation of energy. A clearer picture of the mechanical behavior of rock can be obtained by analyzing the energy fluctuation during mechanical damage. Absorbed energy is the term used to describe the energy required to fracture the specimen. The evaluation of the absorbed energy corresponds to the energy estimation in the experiments on uniaxial compressive strength. The area under stress versus strain curve can be used to determine the absorbed energy, as demonstrated in Figure 2, using Equation 1. After peak loading, residual stresses cause the strain energy to rise steadily, resulting in a continuous increase in the absorbed energy. Even though there may be differences in the numerical values, the energy conversion method remains the same across all loading conditions. The variation in absorbed energy can be explained by four stages of energy conversion. The first stage (compression stage) compresses the existing pores and integral discontinuities under reduced stresses, resulting in lesser energy. In the second elastic stage, the absorbed energy increases gradually as the loading increases. During the third stage, absorbed energy increases, causing micro-cracks to multiply, and

these eventually grow into macro-cracks. As a result, the sample loss strength (Figure 1) and further propagates the fractures during the fourth stage (expansion and fracture). Rock breaking and damage are caused by the sudden release of absorbed energy. The potential of rock fracturing through the primary fracture increases with the amount of absorbed energy. The greater the absorbed energy, the higher the likelihood of new fractures in rock breaking and damage.

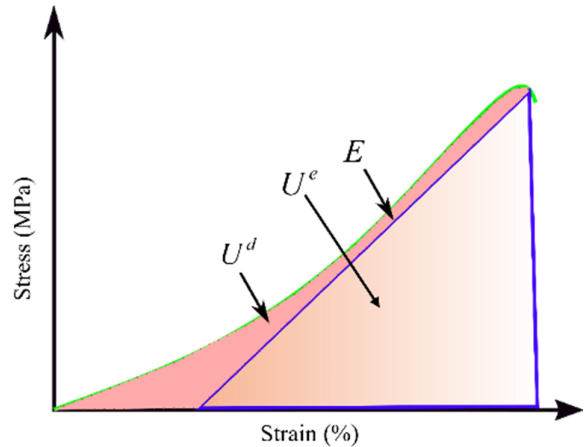


Figure 2. Schematic diagram of elastic energy (U^e), dissipated energy (U^d), and elastic modulus (E) [26].

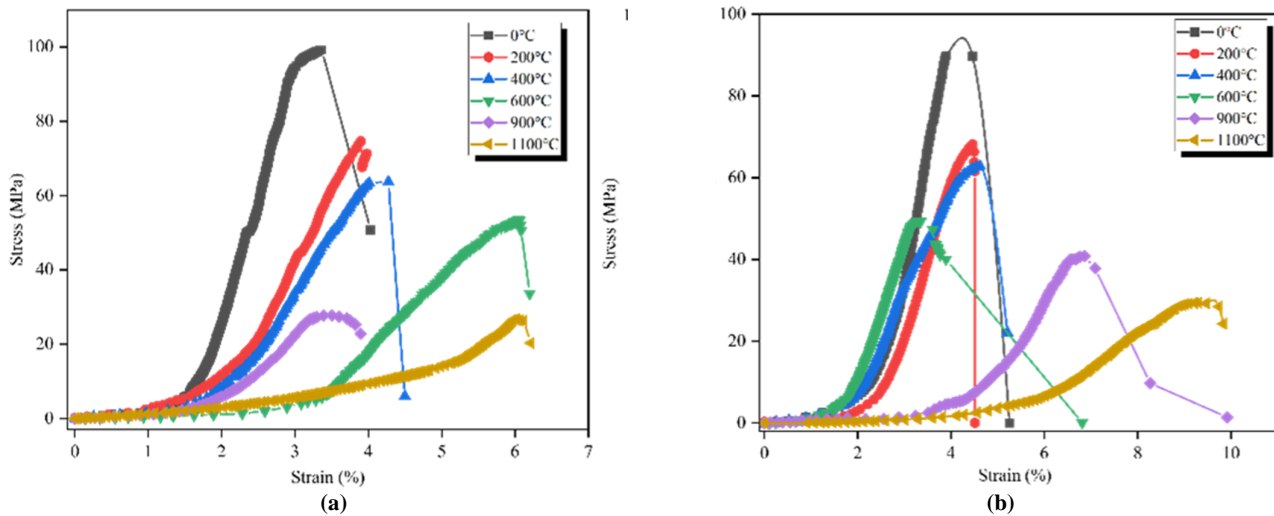


Figure 3. Stress-strain curves of granite rock subjected to uniaxial compression loading at various temperatures (a) pink granite, (b) white-black granite.

3.3. Total energy

The genesis, development, linkage, and sliding of microscopic flaws are all part of the rock deformation and failure process. The formation of new cracks is a result of energy absorption, and the

crack surface dissipates energy during failure. The overall deformation and failure of rock are influenced by both elastic and dissipated strain energy [27, 28]. Figure 4 demonstrates the relationship between total energy and stress for pink and white-black granite under uniaxial

compression at various temperatures. As illustrated in Figure 4, the total energy of both types of granite rock grows linearly as the applied stress increases during the compaction stage, except in the case of pink granite at 0 °C and 1100 °C. Total energy exhibits similar characteristics during the elastic deformation stage. The growth rate of total energy

varies with stress and temperature for each type of granite. As the yield stage is reached, the growth rate of total energy varies, and the overall energy level keeps rising in tandem with the stress. During the failure stage, the total energy of a granite rock exhibits a declining trend with temperature variations.

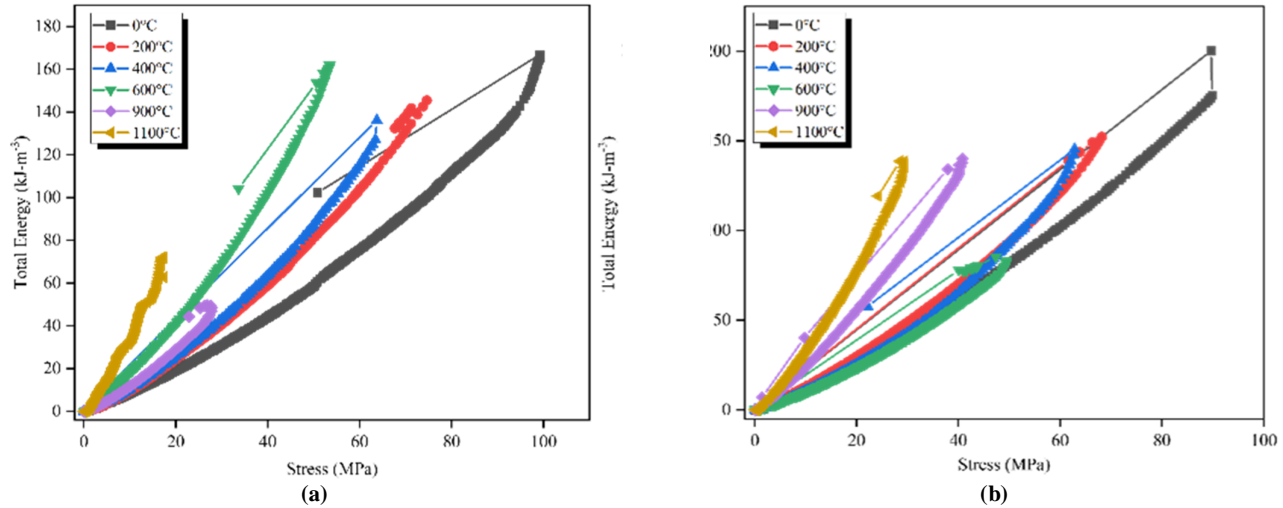


Figure 4. Total energy curves of granite rock subjected to uniaxial compression loading at various temperatures (a) pink granite, (b) white-black granite.

3.4. Elastic energy

Figure 5 depicts the relationship between elastic energy and stress for pink and white-black granite under uniaxial compression at various temperatures. As shown in Figure 5, during the micro-crack compaction stage, the elastic energy barely increases. The reason for this is that the energy required to close micro-flaws is enormous, and only a small fraction of that energy is converted into elastic energy [10]. The rate at which elastic energy grows is at its maximum during the elastic stage, and this rate is proportional to the applied stress. Pink granite heated to 1100 °C shows a non-linear increase in elastic energy. The sustained elastic deformation in the sample caused it, converting a significant portion of energy into elastic energy. Rock cracks began to emerge and widen as the yield stage approached. When the yield stage is reached, the pace of total energy increase changes, and the overall energy level rises in tandem with the stress. The maximum value of elastic energy is exhibited at the peak point, which is 68 kJ/m³ for pink granite and 59 kJ/m³ for white-black granite at room temperature. After absorbing elastic energy, the sample quickly releases this energy, causing pre-existing cracks to widen rapidly and fail the sample.

3.5. Dissipated energy

External forces or stresses cause energy to be dissipated in the form of deformation, fracture or sliding when rocks are subjected to them. Therefore, dissipation energy is the main factor responsible for the internal damage of rocks [29]. Figure 6 shows the relationship between dissipated energy and stress during uniaxial compression at various temperatures for pink and white-black granite. During the compaction stage, the dissipated energy increases exponentially. Based on this, it is inferred that a greater amount of energy is lost during the restructuring process due to the emergence of new fractures and the propagation of pre-existing micro-flaws [10]. The rate of increase of dissipated energy is steady and linear during the elastic stage. The large particle size and high dissipated energy exhibited by both the pink and white-black granite samples demonstrate the instability of this rock [30]. When pink granite is heated to 400 °C and 600 °C, the dissipated energy during the elastic stage initially increases and then decreases. When both samples reach the failure stage, the total amount of energy they have dissipated increases dramatically.

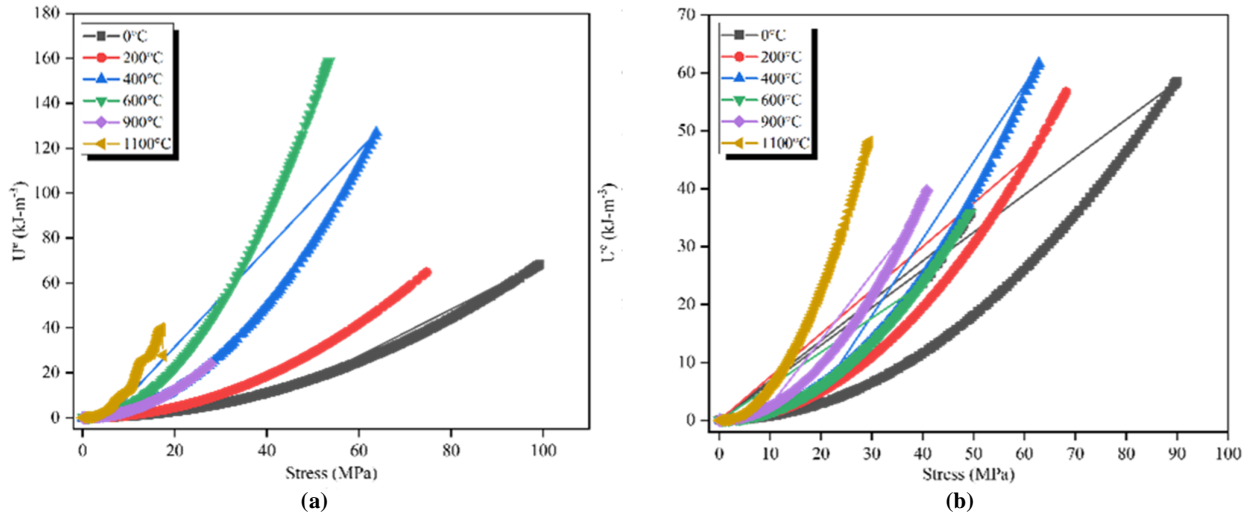


Figure 5. Elastic energy curves of granite rock subjected to uniaxial compression loading at various temperatures (a) pink granite, (b) white-black granite.

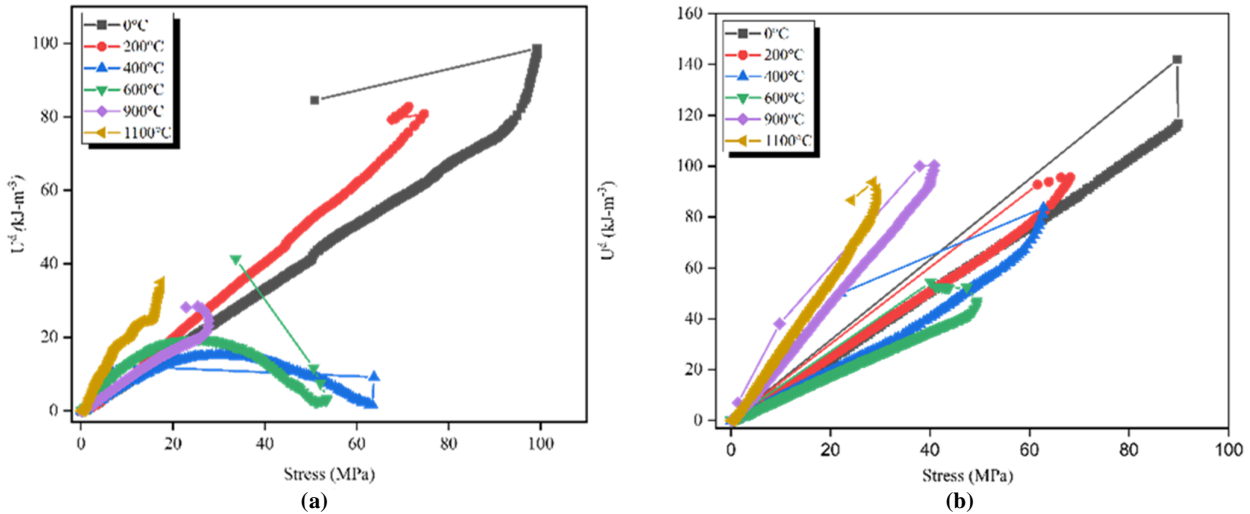


Figure 6. Dissipated energy curves of granite rock subjected to uniaxial compression loading at various temperatures (a) pink granite, (b) white-black granite.

3.6. Dissipation energy coefficient

The ratio of the dissipated energy to the elastic energy is known as the “dissipation energy coefficient”. Figure 7 shows the relationship between dissipated energy coefficient and stress during uniaxial compression at various temperatures for pink and white-black granite. The dissipation energy coefficient undergoes four stages (compaction, elastic deformation, yield, and failure). Figure 8 shows that the dissipation energy coefficient undergoes four separate phases of evolution, marked by three unique characteristic points. Point O to A in Figure 8 represents the compaction stage, also known as the first

characteristic point of the curve. The strength at point A is referred to as compaction strength, and at this stage, the dissipation energy coefficient λ increases rapidly but at a very low rate. This is due to the fact that closing micro-flaws consume the majority of energy during the early phase. The elastic deformation stage (AB) is the second characteristic point of a curve, with point B known as the yield point. The dissipation energy coefficient values decline, albeit at a moderate rate, until they reach the minimal value. Additionally, there is essentially little new crack production or propagation at this point, and energy dissipation is rather minimal. Consequently, there is a drop in the dissipation energy coefficient. The third stage of

the curve is known as the yield stage (BC), with point C as the peak point. At this point, the dissipation energy is constantly increasing because fresh micro-cracks are no longer being formed in the rock. The dissipation energy coefficient increases considerably at the failure stage (CD). This is because, at the failure stage, crack growth

accelerates dramatically, and particle slip increases.

It is also clear that during the four stages, the elastic and dissipated energies go through different "primary" and "secondary" states. The rate of U^d is greater than the rate of U^e throughout the loading.

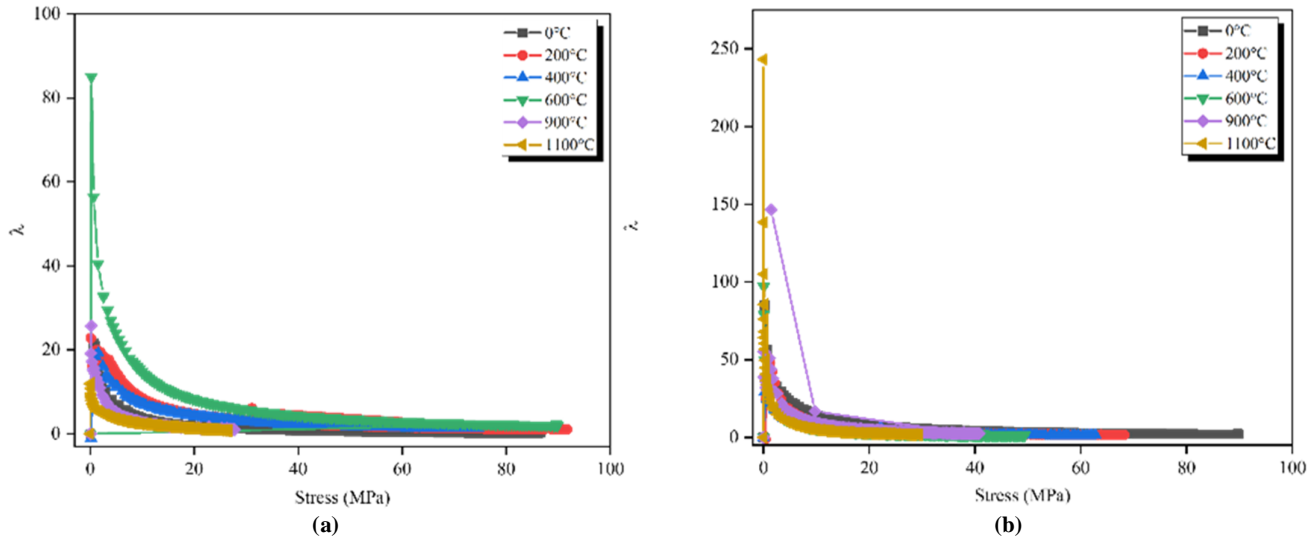


Figure 7. Dissipated energy coefficient variation with the stress of granite rock subjected to uniaxial compression loading at various temperatures (a) pink granite, (b) white-black granite.

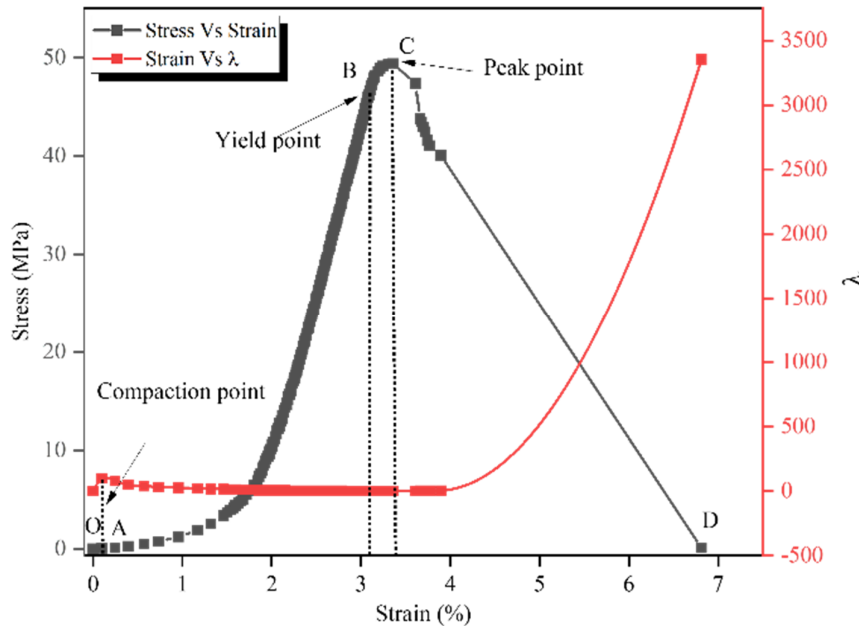


Figure 8. Relationship between strain and dissipated energy coefficient.

The stress-strain relationship can represent rock deformation and failure processes; however, it has some limits in specific areas such as the degree to which the rock sample fails violently when it is loaded. The brittleness index (BIM) described in

Equation 6 is used for this purpose. This index is the ratio of the total energy and the elastic energy [10].

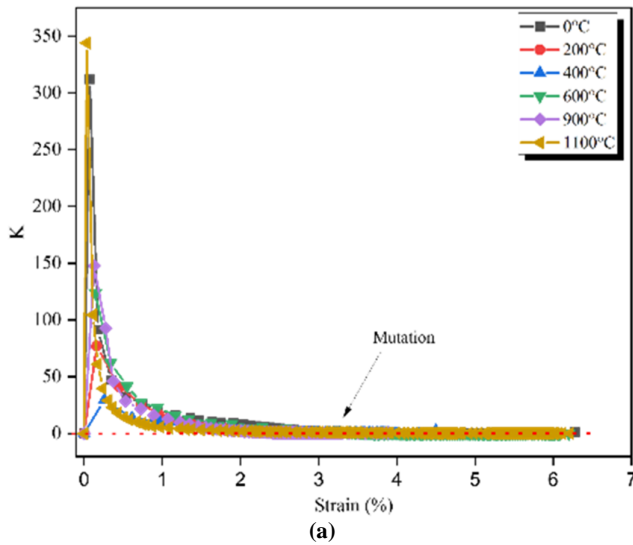
$$BIM = \frac{U}{U^e} \tag{6}$$

where BIM is one of the approaches used to estimate rock burst susceptibility. The evaluation of rock bursting based on the BIM values for rock under-loading is given in Table 3.

All BIM values for pink and white-black granite are both above 1.5, which indicates that the granite samples are susceptible to weak rock bursting. The derivatives of the dissipation energy coefficient with respect to the axial strain determine the rate of change of K, the dissipation energy coefficient, as shown in Figure 9. Equation 7 represents the rate of change of the dissipation energy coefficient.

$$K = \frac{d\lambda}{d\varepsilon} \tag{7}$$

Figure 9 portrays the correlation between the rate of change of dissipated energy coefficient and strain during uniaxial compression at different temperatures for pink and white-black granite. The graph/plot illustrates a mutation E in the rate of change of the dissipation energy coefficient at the end of the compaction stage. Although the K values approach 0, they do not become negative.



4. Failure modes

A total of 36 specimens, consisting of 18 pink granite and 18 white-black granite samples, were tested under uniaxial compression at various temperatures. Figure 10 displays the various failure modes in rock samples under uniaxial compression including axial splitting, shear, multiple fractures (MF), and shear along a single plan (shear S). The results revealed that axial splitting is the predominant mode of failure. The figure also shows the failure modes that can be described based on the rock deformation behavior during uniaxial compression. The occurrence of failure patterns involving multiple fractures in the rock is associated with uniaxial compression, as wing cracks can propagate freely when parallel to the major principal stresses.

Table 3. Evaluation of rock bursting based on the BIM value [10].

BIM value	Rock burst tendency
BIM > 1.5	Weak rock burst
1.2 < BIM ≤ 1.5	Medium rock burst
1.0 ≤ BIM ≤ 1.2	Strong rock burst

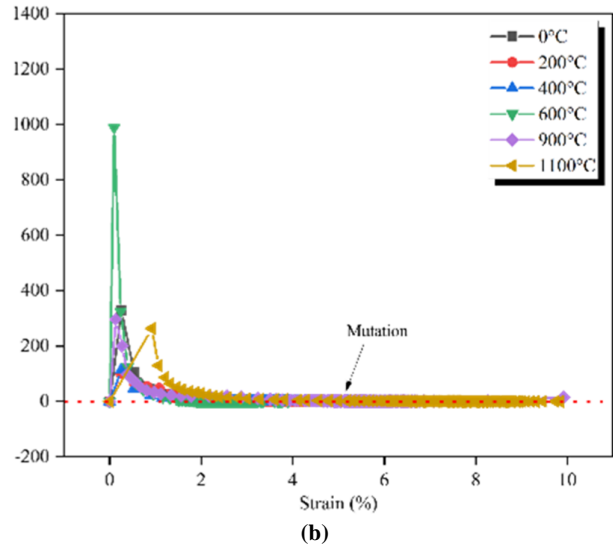


Figure 9. Graph showing the dissipation energy coefficient rate of change (K) (a) pink granite, (b) white-black granite.

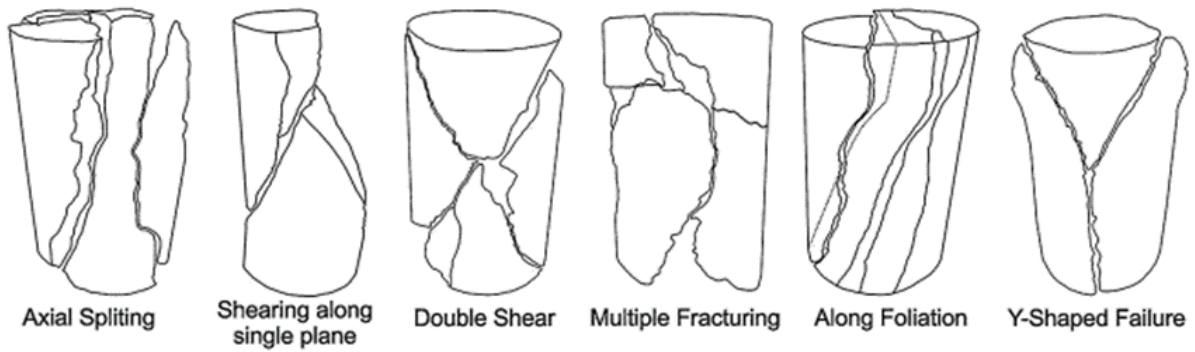


Figure 10. A schematic representation of a specific failure mode of rock specimen under uniaxial compression [16].

As shown in Figure 11, if a pre-existing incipient discontinuity hinders wing crack propagation and the coalescence of horizontal and vertical directional micro-flaws occurs, the specimen fails in the multiple fracturing modes. Under uniaxial compression, multiple fractures are more likely to occur in rock than other types of failure patterns, as wing cracks propagate most clearly when located parallel to the maximum primary stresses. Figure

11(a) illustrates the multiple fracturing modes of a rock specimen. On the other hand, if micro-flaws only hinder the wing cracks in the vertical direction, the rock specimen fails in the axial failure mode, as shown in Figure 11(b). However, if the coalescence of adjacent micro-flaws occurs in the vertical direction or does not impede the wing cracks, the rock specimen fails in the shear failure mode, as shown in Figure 11 (c) [16].

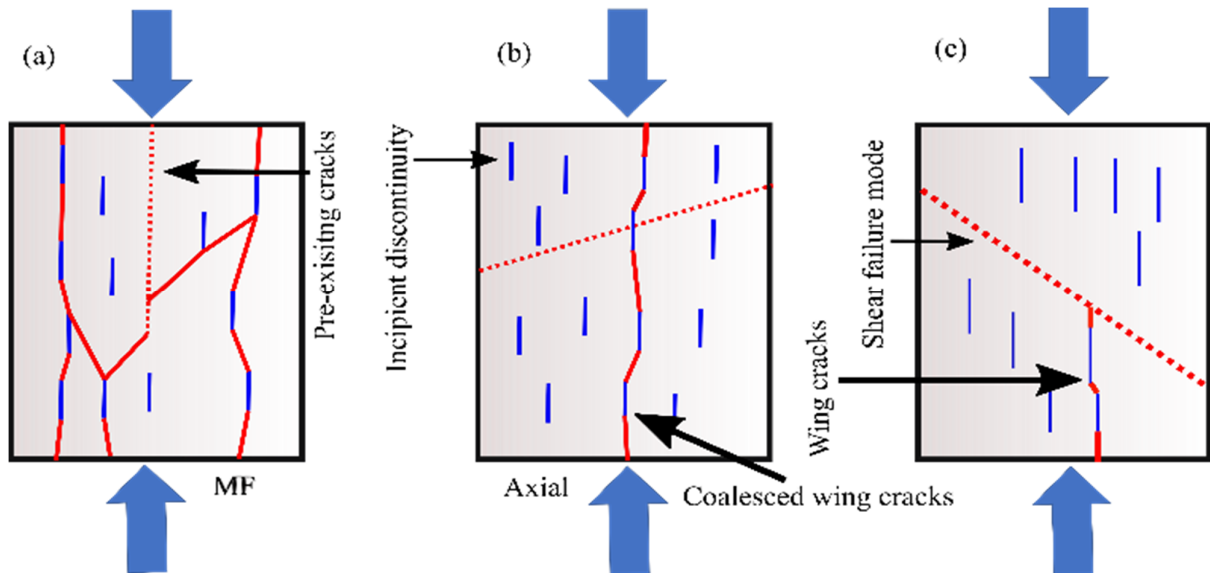


Figure 11. (a) Multiple fractures caused by the coalescence of micro-flaws are responsible for cracks in both the horizontal and vertical directions. (b) Axial splitting occurs as a result of micro-flaws coalescing with vertical wing cracks. (c) When wing cracks do not spread throughout the entire specimen but instead fracture along the shear plane, we have a shear failure [16].

Based on the observations in Figure 12 the failure mode of pink granite is axial splitting, except for specimens subjected to 900 °C, which failed in shear mode. Similarly, white-black granite specimens fail in axial mode, with the exception of

those exposed to 1100 °C, which fail in shear and multiple splitting modes. The results indicated that at higher temperatures, shear and multiple fracture modes were more prevalent than axial splitting.



Figure 12. Failure modes of granite observed under uniaxial compression at different temperatures.

5. Conclusions

The energy principle was utilized to investigate the energy characteristics, failure modes, and dissipation energy coefficient evolution of pink and white-black granite under uniaxial compression at various temperatures. The major conclusions are as follows:

1. The analysis of energy characteristics provides a reliable perspective on rock deformation and failure, particularly the dissipation energy coefficient, which initially increases rapidly and then decreases to a minimum value. The K values remained constant during the failure stage and continued to follow the minimum value.

2. The dissipation energy of white-black granite is greater than elastic energy, likely due to its larger grain size compared to pink granite.
3. Axial splitting was the predominant failure mode observed in the majority of the damaged granite specimens. This is due to the microstructures in the granite rock with larger grain size being unable to hinder the propagation of wing cracks.
4. At temperature up to 600 °C, the impact on regulating the failure mode is significant. However, when heated above 600 °C, the effect manifests as a multiple fractures and shearing failure mode.

References

- [1]. Lei, Y., J. Huang, Y. Cui, S.-H. Jiang, S. Wu, and J. Ching. (2023). Time capsule for landslide risk assessment. *Georisk: Assessment and Management of Risk for Engineered Systems and Geohazards*: 1-22.
- [2]. Holma, M., Z. Zhang, P. Kuusiniemi, K. Loo, and T. Enqvist. (2022). Future prospects of muography for geological research and geotechnical and mining engineering. *Muography: Exploring Earth's Subsurface with Elementary Particles*: 199-219.
- [3]. Shah, K.S., M.H.b.M. Hashim, M.Z. Emad, K.S.b. Ariffin, M. Junaid, and N.M. Khan. (2020). Effect of particle morphology on mechanical behavior of rock mass. *Arabian Journal of Geosciences*, 13: 1-17.
- [4]. Sultan Shah, K., M.H.B. Mohd Hashim, H.U. Rehman, and K.S.B. Ariffin. (2022). Evaluating microscale failure response of various weathering grade sandstones based on micro-scale observation and micro-structural modelling subjected to wet and dry cycles. *Journal of Mining and Environment*, 13(2): 341-355.
- [5]. Shah, K.S., M.H.B. Mohd Hashim, and K.S.B. Ariffin. (2022). Photogrammetry and Monte Carlo Simulation based statistical characterization of rock mass discontinuity parameters. *International Journal of Mining and Geo-Engineering*, 56(2): 151-157.
- [6]. Timchenko, A. and J.-L. Briaud. (2023). ANALYSIS OF A DATABASE OF OPEN-PIT MINE SLOPE FAILURES TO PREDICT TRAVEL DISTANCE, SETBACK DISTANCE, AND GEOMETRIC PROPERTIES. *Canadian Geotechnical Journal*, (ja).
- [7]. He, Y., B. Li, and X. Du. (2023). Soil Slope Instability Mechanism and Treatment Measures under Rainfall—A Case Study of a Slope in Yunda Road. *Sustainability*, 15(2): 1287.
- [8]. Zhang, S., L. Shi, and D. Jia. (2023). An uncertainty quantitative model of wellbore failure risk for underground gas storage in depleted gas reservoir during the construction process. *Journal of Energy Storage*, 57: 106144.
- [9]. Zhang, A., H. Xie, R. Zhang, M. Gao, J. Xie, Z. Jia, L. Ren, and Z. Zhang. (2023). Mechanical properties and energy characteristics of coal at different depths under cyclic triaxial loading and unloading. *International Journal of Rock Mechanics and Mining Sciences*, 161: 105271.
- [10]. He, M., F. Pang, H. Wang, J. Zhu, and Y. Chen. (2020). Energy dissipation-based method for strength determination of rock under uniaxial compression. *Shock and Vibration*, 2020: 1-13.
- [11]. Cao, K., L. Ma, Y. Wu, N. Khan, and J. Yang. (2020). Using the characteristics of infrared radiation during the process of strain energy evolution in saturated rock as a precursor for violent failure. *Infrared Physics & Technology*, 109: 103406.
- [12]. Li, D., Z. Sun, T. Xie, X. Li, and P. Ranjith. (2017). Energy evolution characteristics of hard rock during triaxial failure with different loading and unloading paths. *Engineering Geology*, 228: 270-281.
- [13]. Hemmati, A., M. Ghafoori, H. Moomivand, and G.R. Lashkaripour. (2020). The effect of mineralogy and textural characteristics on the strength of crystalline igneous rocks using image-based textural quantification. *Engineering Geology*, 266: 105467.
- [14]. Hao, Y., Y. Wu, R. Cui, K. Cao, D. Niu, and C. Liu. (2023). Strain Energy Dissipation Characteristics and Neural Network Model during Uniaxial Cyclic Loading and Unloading of Dry and Saturated Sandstone. *Minerals*, 13(2): 131.
- [15]. Fakhimi, A. and B. Hemami. (2015). Axial splitting of rocks under uniaxial compression. *International Journal of Rock Mechanics and Mining Sciences*, 79: 124-134.
- [16]. Basu, A., D. Mishra, and K. Roychowdhury. (2013). Rock failure modes under uniaxial compression, Brazilian, and point load tests. *Bulletin of Engineering Geology and the environment*, 72: 457-475.
- [17]. Nemat-Nasser, S. and H. Horii. (1984). Rock failure in compression. *International Journal of Engineering Science*, 22(8-10): 999-1011.
- [18]. D-08, A. (2008). Standard practices for preparing rock core as cylindrical test specimens and verifying conformance to dimensional and shape tolerances. *Annual Book of ASTM Standards*.
- [19]. Vidana Pathiranagei, S., I. Gratchev, and R. Kong. (2021). Engineering properties of four different rocks after heat treatment. *Geomechanics and Geophysics for Geo-Energy and Geo-Resources*, 7: 1-21.
- [20]. Małkowski, P., P. Kamiński, and K. Skrzypkowski. (2012). Impact of Heating of carboniferous rocks on their mechanical parameters. *AGH Journal of Mining and Geoengineering*, 36(1): 231-142.

- [21]. Yuan, P., D. Tan, F. Annabi-Bergaya, W. Yan, M. Fan, D. Liu, and H. He. (2012). Changes in structure, morphology, porosity, and surface activity of mesoporous halloysite nanotubes under heating. *Clays and Clay Minerals*, 60(6): 561-573.
- [22]. Nahhas, T., X. Py, N. Sadiki, and S. Grégoire. (2019). Assessment of four main representative flint facies as alternative storage materials for concentrated solar power plants. *Journal of Energy Storage*, 23: 79-88.
- [23]. ASTM, D. (1995). 2938, Standard test method for unconfined compressive strength of intact rock core specimens. ASTM International, West Conshohocken, PA.
- [24]. Xie, H., L. Li, R. Peng, and Y. Ju. (2009). Energy analysis and criteria for structural failure of rocks. *Journal of Rock Mechanics and Geotechnical Engineering*, 1(1): 11-20.
- [25]. Zhang, M., Q. Meng, and S. Liu. (2017). Energy evolution characteristics and distribution laws of rock materials under triaxial cyclic loading and unloading compression. *Advances in Materials Science and Engineering*, 2017.
- [26]. Cui, B., G. Feng, J. Bai, G. Xue, K. Wang, X. Shi, S. Wang, Z. Wang, and J. Guo. (2023). Failure characteristics and the damage evolution of a composite bearing structure in pillar-side cemented paste backfilling. *International Journal of Minerals, Metallurgy and Materials*: 1-14.
- [27]. Zhang, Q.B. and J. Zhao. (2014). Quasi-static and dynamic fracture behaviour of rock materials: phenomena and mechanisms. *International Journal of Fracture*, 189: 1-32.
- [28]. Liu, K., T. Guo, J. Yang, and S. Ma. (2023). Static and dynamic fracture behavior of rock-concrete bi-material disc with different interface crack inclinations. *Theoretical and Applied Fracture Mechanics*, 123: 103659.
- [29]. Taheri, A., N. Yfantidis, C. Olivares, B. Connelly, and T. Bastian. (2016). Experimental study on degradation of mechanical properties of sandstone under different cyclic loadings. *Geotechnical Testing Journal*, 39(4).
- [30]. Gao, L., F. Gao, Z. Zhang, and Y. Xing. (2020). Research on the energy evolution characteristics and the failure intensity of rocks. *International Journal of Mining Science and Technology*, 30(5): 705-713.

تجزیه و تحلیل حالت‌های شکست گرانیت و تبدیل انرژی تحت فشرده سازی تک محوری در دماهای مختلف

کوثر سلطان شاه^{1*}، نعیم عباس^{1,2}، لی کگانگ²، محد حزیزان بن محد هاشم³، حافظ الرحمن^{3,4} و خان گل جادون¹

1. گروه مهندسی معدن، دانشگاه بین المللی قراقرام (KIU)، گیلگیت، پاکستان

2. دانشکده مهندسی منابع زمین، دانشگاه علم و فناوری کونمینگ، کونمینگ، یونان، چین

3. دانشکده مهندسی مواد و منابع معدنی، دانشگاه ساینس مالزی، پردیس مهندسی، نیبونگ تبال، پنانگ، مالزی

4. گروه مهندسی معدن، دانشگاه فناوری اطلاعات بلوچستان، علوم مهندسی و مدیریت، کوئته، پاکستان

ارسال 2023/03/23، پذیرش 2023/04/30

* نویسنده مسئول مکاتبات: kausar.sultan@kiu.edu.pk

چکیده:

سنگ‌های منطقه مورد مطالعه به دلیل قرار گرفتن مکرر در معرض تغییرات شدید دما و شرایط بارگذاری مستعد تخریب و شکست هستند. در زمینه ارزیابی قابلیت اطمینان مهندسی سنگ، درک فرآیند تبدیل انرژی در سنگ‌ها بسیار مهم است. بنابراین، این کار تحقیقاتی با هدف ارزیابی ویژگی‌های انرژی و حالت‌های شکست گرانیت صورتی و سفید-سیاه تحت بارگذاری فشاری تک محوری در دماهای مختلف انجام می‌شود. نمونه‌های گرانیت صورتی و سفید-سیاه تا طیف وسیعی از دماها (0 درجه سانتیگراد، 200 درجه سانتیگراد، 400 درجه سانتیگراد، 600 درجه سانتیگراد، 900 درجه سانتیگراد و 1100 درجه سانتیگراد) گرم می‌شوند و حالت‌های خرابی و ویژگی‌های انرژی آنها شامل انرژی کل، انرژی الاستیک و انرژی تلف شده با آزمایش نمونه‌های پیش گرم شده تحت فشار تک محوری مورد مطالعه قرار می‌گیرند. نتایج نشان می‌دهد که ضریب اتلاف انرژی در ابتدا به سرعت افزایش می‌یابد و سپس در مرحله شکست به حداقل مقدار خود باز می‌گردد. ریزساختارهای سنگ گرانیت مستقیماً بر انرژی الاستیک و اتلاف آن تأثیر می‌گذارد. حالت شکست تقسیم محوری در اکثر نمونه‌های گرانیت آسیب دیده مشاهده می‌شود. پس از حرارت دادن گرانیت تا دمای 600 درجه سانتیگراد، تأثیر دما بر حالت خرابی آشکار می‌شود.

کلمات کلیدی: حالت شکست، گرانیت، انرژی تلف شده، انرژی الاستیک، تقسیم محوری.